THE INTERPLAY BETWEEN SPATIALLY SEPARATED FERROMAGNETIC AND SUPERCONDUCTING THIN FILMS

A Senior Honors Thesis

by

ISAAC JOHN SULLIVAN

Submitted to the Office of Honors Programs & Academic Scholarships
Texas A&M University
in partial fulfillment of the requirements of the

UNIVERSITY UNDERGRADUATE RESEARCH FELLOWS

April 2001

Group: Physical Sciences

THE INTERPLAY BETWEEN SPATIALLY SEPARATED FERROMAGNETIC AND SUPERCONDUCTING THIN FILMS

A Senior Honors Thesis

by

ISAAC JOHN SULLIVAN

Submitted to the Office of Honors Programs & Academic Scholarships
Texas A&M University
in partial fulfillment for the designation of

UNIVERSITY UNDERGRADUATE RESEARCH FELLOW

Approved as to style and content by:

Donald G. Naugle
(Fellows Advisor)

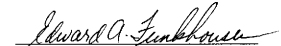

Edward A. Funkhouser
(Executive Director)

April 2001

Group: Physical Sciences

ABSTRACT

The Interplay between Spatially Separated Ferromagnetic and Superconducting Thin Films. (April 2001)

Isaac John Sullivan

Department of Physics

Texas A&M University

Fellows Advisor: Dr. Donald G. Naugle

Department of Physics

Ferromagnetic thin films have been grown via physical vapor deposition utilizing the technique of flash evaporation and characterized by measuring magnetization as a function of magnetic field. An Al thin film was evaporated atop the ferromagnetic thin film and allowed to oxidize in order to produce a thin insulating layer. Finally, two superconducting thin films of nearly equal thickness were evaporated via physical vapor deposition onto the Al_2O_3 insulating layer. Both superconducting films, one coupled magnetically, but not electrically, with the ferromagnetic thin film and the other isolated, were studied by measuring resistivity as a function of temperature in various magnetic fields between 0 G and 2 kG. It was found that the effect of the ferromagnetic thin film decreased the superconducting resistive transition width, or equivalently, that the flux flow resistance has been reduced.

To Cecelia S. Pellegrini and Lovey Christine Matragrano

ACKNOWLEDGMENTS

Many people deserve thanks and recognition for the undertaking of this work. The sincerest thanks to Professor Naugle for the opportunity to work in his laboratory. His encouragement and guidance throughout my college career made this work possible. Visiting Professor Anil Bhatnagar deserves special thanks for teaching me the experimental physics necessary to carry out much of the work described in this thesis. I truly feel blessed to have worked with such a gentlemen and scholar. Dr. Daya Rathnayaka deserves appreciation for his gratuitous answers to my endless questions. My gratitude towards him is indescribable. Thanks are due Aaron C. DuMar, Jim M. Eyhorn, and Brian D. Hennings for all of their assistance. I would like to thank Jennifer N. Barron and my family for all of their love and support. Lastly, I give glory to my Lord and Savior Jesus Christ for the purchase of my life with His death and resurrection.

TABLE OF CONTENTS

LIST OF TABLES

LIST OF FIGURES

FIGURE Page

FIGURE Page

FIGURE Page

CHAPTER I

INTRODUCTION

In 1911, H. Kamerlingh-Onnes observed that the electrical resistance of mercury drops to zero very rapidly at a temperature of 4.5 K [1]. The discovery of superconductivity opened the doorway to intense theoretical and experimental inquiry. One such interesting aspect of study is the interplay between superconductivity and ferromagnetism. Both are long range order phenomena that heavily compete against one another.

Two different types of superconductors exist, those being type I and type II, respectively. Type I superconductors expel all magnetic flux up to a certain critical field, denoted by H_c. The critical temperature T_c is defined as the temperature at which a material goes superconducting, *i.e.* there is no measureable DC electrical resistance. For $T < T_c$, a type I superconductor expels the magnetic field up to a distance λ_L, known as the London penetration depth. Meissner and his graduate student Ochsenfeld verified experimentally that if a normal metal in a magnetic field is cooled below T_c, the magnetic flux is expelled completely up to a distance λ_L. Physically, as a material's temperature drops below the critical temperature, surface currents are generated that exactly cancel out the magnetic field inside the material. For an applied magnetic field greater than the critical field H_c, it is energetically favorable for the field to penetrate the material, thus destroying superconductivity. Type II superconductors are similar to type I superconductors in that below the lower critical field, denoted by H_{c1}, perfect diamagnetism is displayed. Likewise, for magnetic fields above the upper critical field H_{c2}, superconductivity is destroyed. However, for fields $H_{c1} < H < H_{c2}$, the material is in what is called the vortex state. In this state, the magnetic field partially penetrates the material in the form of thin filaments of

---

The journal model is *Physica C: Superconductivity.*

magnetic flux [2]. Within each filament of flux, the material is in its normal state; whereas, outside the filament the material remains superconducting. A superconducting vortex, or supercurrent, also accompanies each flux tube. Experiments [3], [4] have proven that each supercurrent in a type II superconductor allows one flux quantum. The value of the flux quantum is $\phi_0 = hc/2e = 2.0679 \times 10^{-7}$ G-cm^2, where h is Planck's constant, c is the speed of light, and e is the charge of the electron. One can thus imagine a type II superconductor in the vortex state as a birthday cake. Each candle represents a normal region of the cake and each wick inside a candle represents the single magnetic flux line that penetrates the cake.

In 1957, Bardeen, Cooper, and Schrieffer proposed a microscopic theory of superconductivity [5]. Commonly referred to as the BCS theory, it proposed that electrons near the Fermi surface experience a net attraction and form into what are known as Cooper pairs when the temperature falls below the critical temperature. This seems counterintuitive given the Coulomb repulsion of two negatively charged particles; however, it is understood through electron-phonon interactions. Phonons, or lattice vibrations, are induced when an electron scatters from a positive ion core in a crystal lattice. Because the electron and positive ion core have opposite charges, the positive ion core is attracted to the electron and vice-versa, but since the positive ion is so much heavier than the electron, its position distorts only slightly, whereas the electron has scattered far away. Since a net positive charge now exists in the place where the ion has moved, another passing electron feels this positive charge and is attracted to its position, thus changing its direction of motion. This creates an overall net attraction between electrons that are far enough apart. Each Cooper pair forms a singlet state where the electrons have equal and opposite momentum or wave vectors. The fact that the electrons form into pairs explains why a factor of 2 appears in the denominator of the expression for the magnetic flux quantum ϕ_0. Another important length scale for type II superconductors is called the coherence length, denoted by ξ. This length is the mean

distance between electrons in a Cooper pair and the length over which the properties of a superconductor can change drastically. Thus the two important length scales that describe a superconductor are the London penetration depth λ_L and the coherence length ξ.

Picture a constant DC current flowing through a type II superconductor that is in the vortex state. Because $H_{c1} < H < H_{c2}$, the material is threaded with the magnetic field lines associated with the normal cores. The current interacts with these magnetic field lines via the Lorentz force. This force drags the superconducting vortices in the direction of the force. As the supercurrents move, they drag their flux lines. According to Faraday's Law, a changing magnetic flux induces a voltage. Mathematically, $\varepsilon = -d\phi/dt$, where ε is the generated voltage, ϕ is the magnetic flux, and $-d/dt$ denotes differentiation with respect to time. As the supercurrents are driven across the material, a voltage appears and a resistance is generated. This resistance is coined flux flow resistance. The appearance of flux flow resistance destroys the zero resistance environment characteristic of superconductors. A solution to the problem of flux flow resistance is to introduce mechanisms into the material, such as defects or imperfections, that effectively pin the supercurrents, rendering them immobile.

The interplay of superconductivity and ferromagnetism has interested both theoretical and experimental physicists for quite some time [6], [7]. When both order parameters are homogeneous in space, ferromagnetism and superconductivity suppress one another due to the proximity effect and spin diffusion [8]. Physically, this is understood in terms of the strong spin scattering of the ferromagnetic impurities with the two oppositely paired momentum electrons of a Cooper pair [9]. Each electron in the pair experiences a different interaction with the ferromagnetic impurity, thus breaking the pair and destroying superconductivity.

Although unavoidable for superconducting/ferromagnetic (SC/FM) systems that are homogeneous in space, separating these two systems in space allows their mutual coex-

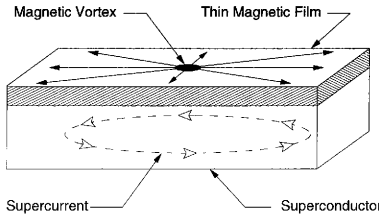

Fig. 1. Interaction of superconducting and magnetic vortices. Figure courtesy A. C. DuMar.

istence [10]. Imagine the interaction of a supercurrent in a superconducting film with the magnetization of a homogeneous magnetic film. Let the superconducting film and the magnetic film be separated by a thin oxide barrier. Lyuksyutov, Naugle, and Pokrovsky [8] have suggested that this configuration would result in the pinning of supercurrents that exist in the vortex state of a type II superconductor. The pinning mechanism occurs via the interaction between the radial component of the magnetic flux due to the supercurrent and the radial magnetic flux of the induced two-dimensional magnetic vortex. Figure 1 depicts this scenario. The pinning of supercurrents would result in a decrease in the flux flow resistance.

The purpose of this thesis was to measure the flux flow resistance for the SC/FM configuration described above in order to determine if the presence of the ferromagnetic thin film reduced the flux flow resistance by pinning supercurrents. This was accomplished by evaporating a ferromagnetic thin film via physical vapor deposition onto a quartz substrate. Aluminum is then evaporated atop the ferromagnetic thin film and oxidized to produce an Al_2O_3 insulation layer. Finally, two superconducting thin films are evaporated onto the Al_2O_3 barrier. Ferromagnetic thin films are subsequently characterized by measuring magnetization as a function of magnetic field using a SQUID magnetometer. Characterization

of the superconducting thin films consisted of measuring resistance as a function of temperature. The superconducting/magnetic thin film multilayer is then compared to an isolated superconductor of the same thickness in order to determine if the flux flow resistance has been reduced.

CHAPTER II

EXPERIMENTAL DETAILS

The preparation and characterization of thin films is of great importance from an experimental perspective. Thin film preparation techniques include physical vapor deposition, electrodeposition, cathode sputtering, and chemical deposition [11]. The characterization of thin films varies widely with the type of film. For example, measuring magnetization as a function of applied magnetic field is extremely useful in characterizing magnetic thin films. All of the films described in this thesis were fabricated via physical vapor deposition. Physical vapor deposition involves the production of a vapor by physical means and allowing the resulting vapor to impinge on a substrate, thus forming a thin film [12]. Resistive heating provided the physical means by which all of the films were evaporated.

Every evaporation occurred in a large stainless steel bell jar. It is approximately 25" in outer diameter, 30" in total length, and with a 0.25" wall thickness, with a somewhat tapered dome welded to the top. A 4" sight glass is positioned on the side of the bell jar so that evaporations are viewable. The bell jar stands next to a metal case which contains three power supplies that provide the current necessary to evaporate different materials. Both the bell jar and metal case are mounted on a huge blue pumping station furnished by the United States Navy. The pumping station houses a water cooled oil diffusion pump which is backed by a two stage mechanical pump, as seen in Figure 2. A liquid nitrogen trap allows the system to reach pressures of approximately $8 - 9 \times 10^{-7}$ torr, as determined by a Granville-Phillips Ionization Gauge, Model 274013. The addition of Marsh beaded heaters yields pressures of $\sim 2 \times 10^{-7}$ torr after baking the system at least 20 hours.

Because fingerprints can introduce unwanted residues in any vacuum system, exacting measures were implemented when preparing for an evaporation. Cloth or latex gloves were always worn when working inside the bell jar. Any items needed for the setup of an

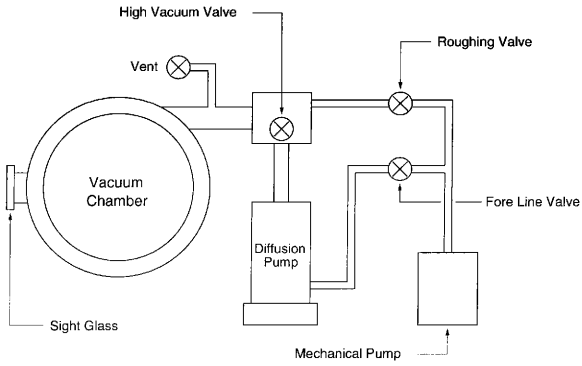

Fig. 2. Schematic of the vacuum system.

evaporation were properly cleaned with acetone followed by alcohol in order to remove any greases or residues. As my project progressed I became increasingly clean with the vacuum chamber and everything associated with it. As a result the system attained pressures of $\sim 1 - 3 \times 10^{-7}$ torr.

I fabricated all of the films on either glass or quartz substrates. Since microscope slides are relatively inexpensive and easy to attain, they were primarily used. When quartz slides were available, they were used as well. Both serve as quality substrates because both surfaces are smooth on a scale comparable to the film thickness [11]. All of the substrates were cut to the appropriate dimensions using an Isomet diamond saw. The substrates were then cleaned by being subjected to fifteen minutes of ultrasonic agitation in a mixture of Micro solution and deionized water, followed by fifteen minutes of ultrasonic agitation in deionized water, then finally being rinsed with acetone and alcohol. Properly cleaning and

carefully handling the substrates resulted in better quality films.

Two general types of thin films were investigated, those being ferromagnetic and superconducting, respectively. It is important to characterize each individually in order to fully understand their interactions in the SC/FM thin film system.

A. Ferromagnetic Thin Films

The thesis work started with the preparation and characterization of ferromagnetic thin films. Ferromagnetic films constituted approximately 80% of the total number of films evaporated. The reason for this is that a multitude of extra films were evaporated in order to accumulate data for a contributed paper delivered at the Joint Meeting of the Texas Section of the American Physical Society, Texas Section of the American Association of Physics Teachers, Society of Physics Student, Zone 13, and the National Society of Hispanic Physicists, at Rice University. Compared to evaporating the oxide barrier or the superconducting thin films, fabricating the ferromagnetic thin films required the most time. The explanation for this is that the technique used to evaporate the films, known as flash evaporation, which will be described in the next section, demands more time for both the setup and the evaporation.

1. Film Preparation

The elements Co and B comprised the ferromagnetic alloys used to fabricate the majority of thin films. Although many different atomic percentages were tested, $Co_{61}B_{39}$ displayed the low coercive fields desired for the SC/FM multilayer system.

Making the $Co_{61}B_{39}$ alloy consisted of combining pure Co and B, 99.9% and 99.7%, respectively, into the appropriate atomic proportions. Johnson Matthey Electronics supplied the Co and Aldrich Chemical Co. supplied the B. The separate pieces of Co and B

were then melted and remelted in an Ar arc furnace in pressures of approximately $12-15$" Hg. If the resulting alloy appeared to be nonuniform, then remelting occured. Weighing the alloy between each melt allowed me to monitor the material loss to ensure that the atomic percentages were not drastically altered. Boron loss is a primary concern because during the initial melting of every CoB alloy made, the small pieces of B would fly all over the chamber every time the arc hovered over the material due to the fact that B is so light. I tried to resolve this problem by only using large chunks of B, but this attempt proved unsuccessful because of the porous nature of B. I would successfully heat up a large chunk of B only to watch it explode into a multitude of pieces all over the chamber because it would release trapped gases. Performing many melts per alloy successfully solved this tedious problem. After making the appropriate alloy, the alloy was crushed into tiny particles and ferromagnetic thin film evaporations could begin.

Because the melting temperatures of Co and B, 1495°C and 2100°C, respectively, differ by such a large amount, evaporating them in large quantities would result in a nonuniform film. Using the technique of flash evaporation overcomes this problem by evaporating tiny particles of the material. The basic idea is that since each particle is so small, it evaporates instantaneouly, or "flashes" into a vapor that ultimately impinges on the substrate surface. By evaporating so quickly and not allowing the Co to evaporate first, a uniform film is produced. All of the CoB alloys were evaporated using this technique.

The bell jar contained all of the necessary components to flash evaporate materials. Any special parts needed were machined prior to the beginning of my investigation of thin films. After the alloy, or sample, is crushed into tiny pieces, each individual particle is placed into one of the holes of the stainless steel slider shown in Figure 3.

The amount of material I place in the stainless steel slider depends on how thick of a film I wish to fabricate. Figure 4 depicts the object on which the stainless steel slider rests. This object, referred to as the slider holder, provides a track for the slider to travel.

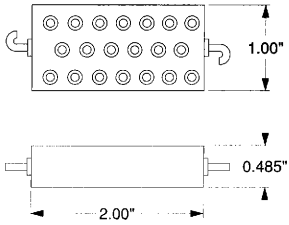

Fig. 3. Scale drawing of the stainless steel slider that holds the particles to be flash evaporated.

The slider holder is mounted on a small rectangular plate with two #8-32 screws and is subsequently attached to a rod that extends into the bottom of the bell jar.

This allows the bottom of the slider holder to lie approximately 12" above the base of the evaporator. A twisted pair of fine steel wire is looped around one of the hooks on the slider and stretched around the two pulleys on the slider holder (see Figure 4). It is then extended to a rotating rod that lies directly in line with the position of the slider. It is important to note that this rotating rod is connected to a feedthrough that can be manually turned from outside the bell jar without introducing an air leak into the vacuum. After being wrapped around the rod two or three times, the remaining portion of the wire is extended back to the unoccupied hook on the slider. The addition of a spring to this end of the wire allows one to adjust the tension in the string and attach the wire to the hook with greater ease. Attached to the bottom of the slider holder is a cone-shaped brass piece that clamps a curved Cu hollow rod with a #2-56 set screw. The opposite end of the Cu rod lies just above a W boat with dimensions 3.5" $\times$ 0.5". After properly aligning the end of the Cu rod over the 0.125" deep dimple of the W boat, two glass rectangular substrates approximately 0.5" $\times$ 0.175" are glued to an Al substrate holder using dilute GE varnish. In addition, two

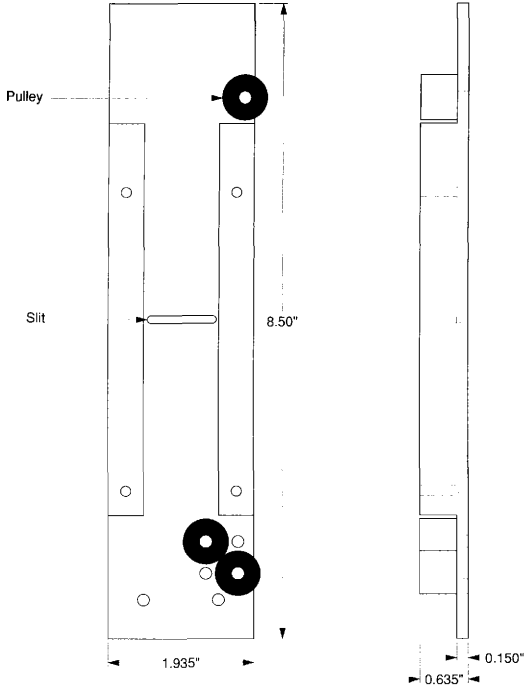

Fig. 4. Scale drawing of the stainless steel slider holder.

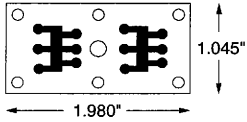

Fig. 5. Scale drawing of the mask used in patterning films for resistance measurements. This film pattern is typically used for both resistance and Hall effect measurements.

0.5" × 0.5" glass substrates are placed on the brass mask displayed in Figure 5.

The Al subsrate holder is then suspended from the upper round plate of the evaporator. It rests approximately 7.5" above the dimple of the W boat. Once the Al substrate holder is mounted securely, the system is closed and pumping begins. The initial flash evaporation procedure, which includes taking out a previously made film and preparing for a new evaporation, takes about one hour.

It initially takes about ten minutes to pump down to a pressure on the order of 10^{-3} torr. At this point, the diffusion pump is allowed to pump on the chamber and the heater beads become operational. The primary reason this investigation required so much time involved having to wait for such a large chamber to reach adequate base pressures. On average, it took approximately one day to fabricate one set of films. When a pressure on the order of 10^{-7} torr is attained, the flash evaporation can begin. Before turning on the power supply, the chilled water valves are opened so that the Cu current feedthroughs do not overheat. I usually passed a current of approximately 300 A through the W boat when evaporating CoB alloys. With such a high current, the W boat glows bright orange and the evaporation is easily seen through the sight glass. As the W boat glows brightly, the handle connected to the rotating feedthrough is turned. The stainless slider begins to traverse the track of the slider holder. When a hole in the slider crosses over the slit in the slider holder (see Figure 4), the material drops into the cone-shaped brass piece, travels down the hollow

Cu rod, and lands in the dimple of the heated W boat, only to be flash evaporated. This process is repeated for however many holes are filled with material or until the desired film thickness is reached.

Film thickness is determined by an Inficon XTM quartz crystal monitor. This device exploits the thickness-frequency relationship of materials deposited onto the quartz substrate. As material impinges onto the quartz crystal, the resonant frequency of the crystal changes. This change in resonant frequency is directly propertional to a change in thickness [13]. The XTM quartz crystal monitor requires three important values in order to calculate the film thickness correctly. These are density of the material (ρ), Z-ratio, and tooling factor. Density refers to the mass of a material divided by its volume. For the XTM crystal monitor, it is measured in units of g/cm^3. The Z-ratio is the acoustic impedence ratio that relates the different elastic properties of materials to the different frequency-thickness relations [13]. Many Z-ratios are listed in Reference [13]. Tooling is the factor that correctly adjusts for the difference in distance between the substrates and the quartz crystal detector. For all of the ferromagnetic thin films produced, $\rho = 7.47$ g/cm^3, Z-ratio = 0.381, and tooling = 100.0.

Because the distance between the substrates and the W boat is different than the distance between the substrates and the quartz crystal detector, a scale factor is calculated in order to determine the actual film thickness. If the substrates are closer to the W boat, then obviously they will have a larger thickness than that determined by the crystal monitor. After a film is fabricated, the crystal monitor reading is recorded and then multiplied by a scale factor to get an estimate on the actual film thickness. We can assume that the evaporated material is a spherical shell of radius R with thickness dR at the point of contact with the substrates and a spherical shell of radius R' with thickness dR' at the point of contact with the quartz crystal detector. By looking at a slice of the two-dimensional projection of the sphere, it is easy to see that in any one slice, the mass of the material should be the same at

both points R and R'. If the density of the material is ρ, we have $2\pi\rho R^2 dR = 2\pi\rho R'^2 dR'$. A 2π instead of a 4π is present because the W boat only allows material to evaporate in the upper half of the sphere. This yields

$$\frac{R'^2}{R^2} = \frac{dR}{dR'}.$$

For evaporating ferromagnetic thin films, the measured distances are $R' \approx 11.3$" and $R \approx 6.9$", thus

$$\frac{dR}{dR'} \approx \left(\frac{11.3}{6.9}\right)^2 \approx 2.7.$$

This shows that a factor of approximately 2.7 must be multiplied by the measurement recorded by the quartz crystal monitor to retrieve the approximate film thickness. The scale factor of ≈ 2.7 is the most frequently used scale factor; however, it does vary from evaporation to evaporation depending on the distance between the boat and the substrates.

After learning how to successfully evaporate ferromagnetic thin films using the technique of flash evaporation, my production of them dramatically increased. Table I shows some of the characteristics of the ferromagnetic thin films fabricated. With the exception of the Al-Gd films and the films containing small impurities of Al and Ge, all of the films were Co_xB_{1-x} alloys. Once a ferromagnetic thin film is made, it must be characterized in order to determine its properties.

Table I. Different characteristics of ferromagnetic thin films. $\approx t$ is the approximate thickness of the film, RT indicates that the substrates were at room temperature during evaporation, LNT indicates that the substrates were at liquid nitrogen temperature during evaporation.

Alloy	Film	Base Pressure (torr)	$\approx t$ (Å)	RT	LNT
$Co_{61}B_{39}$	A1	6.4×10^{-7}	1000	yes	no
$Co_{61}B_{39}$	A2	7.0×10^{-7}	380	yes	no
$Co_{61}B_{39}$	A3	1.3×10^{-6}	250	yes	no
$Co_{61}B_{39}$	A4	1.3×10^{-6}	500	yes	no
$Co_{61}B_{39}$	A5	7.0×10^{-7}	1530	yes	no
$Co_{61}B_{39}$	A6	1.8×10^{-5}	580	yes	no
$Co_{61}B_{39}$	A7	7.8×10^{-7}	3100	yes	no
$Co_{61}B_{39}$	A8	6.5×10^{-7}	240	yes	no
$Co_{61}B_{39}$	A9	6.3×10^{-7}	1120	yes	no
$Co_{61}B_{39}$	A10	4.9×10^{-7}	1800	yes	no
$Co_{61}B_{39}$	A11	3.7×10^{-7}	1930	no	yes
$Co_{61}B_{39}$	A12	5.2×10^{-7}	600	no	yes
$Co_{61}B_{39}$	A13	6.6×10^{-7}	2000	no	yes
$Co_{61}B_{39}$	A14	6.2×10^{-7}	1650	yes	yes
$Co_{61}B_{39}$	A15	5.4×10^{-7}	1250	yes	yes
$Co_{61}B_{39}$	A16	5.4×10^{-7}	260	yes	yes
$Co_{61}B_{39}$	A17	4.5×10^{-7}	785	yes	no
$Co_{61}B_{39}$	A18	6.0×10^{-7}	580	yes	no
$Co_{61}B_{39}$	A19	5.4×10^{-7}	490	yes	no
$Co_{61}B_{39}$	A20	7.2×10^{-7}	250	yes	no

Table I Continued

Alloy	Film	Base Pressure (torr)	$\approx t$ (Å)	RT	LNT
$Co_{61}B_{39}$	A21	7.6×10^{-7}	175	yes	no
$Co_{61}B_{39}$	A22	2.0×10^{-6}	2050	yes	no
$Co_{61}B_{39}$	A22	2.0×10^{-6}	2050	yes	no
$Co_{61}B_{36}Al_3$	B1	6.3×10^{-7}	2200	yes	no
$Co_{61}B_{36}Al_3$	B2	5.7×10^{-7}	1350	yes	no
$Co_{59}B_{41}$	C1	8.0×10^{-7}	340	yes	no
$Co_{59}B_{41}$	C2	1.1×10^{-6}	440	yes	no
$Co_{59}B_{41}$	C2/1	8.0×10^{-7}	780	yes	no
$Co_{59}B_{41}$	C3	6.9×10^{-7}	1070	yes	no
$Co_{59}B_{41}$	C4	2.5×10^{-6}	510	yes	no
$Al_{90}Gd_{10}$	AG-1A	4.4×10^{-7}	1640	yes	no
$Gd_{77}Al_{23}$	AG-2A	4.7×10^{-7}	1230	yes	no
$Al_{85}Gd_{15}$	AG-3A	5.8×10^{-7}	1420	yes	no
$Al_{95}Gd_5$	AG-4A	5.7×10^{-7}	730	yes	no
$Al_{95}Gd_5$	AG-4B	5.1×10^{-7}	1590	yes	no
$Co_{61}B_{34}Ge_5$	G1	5.9×10^{-7}	1990	yes	no
$Co_{61}B_{34}Ge_5$	G2	4.2×10^{-7}	2060	yes	no

2. Film Characterization

Characterization of the ferromagnetic thin films was accomplished by measurement of the magnetization as a function of applied magnetic field. This type of measurement results in a hysteresis curve or loop. The propensity of a ferromagnetic material to resist a change in the magnetic state [11] causes the phenomenon of hysteresis.

The Texas A&M University Chemistry Department's Quantum Design Magnetic Property Measurement System (MPMS) was used to measure the hysteresis for all of the samples. Quantum Design's MPMS houses a superconducting magnet that can reach magnetic fields of 8 T. It also allows for measurements in the temperature range $1.7\ \mathrm{K} \leq T \leq 400\ \mathrm{K}$. The power of the MPMS lies in its ability to sensitively measure magnetization. It does this via a Superconducting Quantum Interference Device (SQUID) detector. Designed to reject the uniform field from the superconducting magnet to a precision of approximately 0.1%, the SQUID detector is insensitive to drifts in the magnet [14], thus allowing better measurements.

All of the films subjected to hysteresis measurements were those evaporated on glass or quartz substrates approximately $0.5" \times 0.175"$. These dimensions are chosen according to the size of sample that the MPMS sample holder can accomodate. The sample holder is a clear plastic drinking straw. Once the sample is inserted into a tiny plastic bag, it can be placed into the drinking straw approximately midway between the two ends. Because I experienced problems with the sample moving within the straw, I began to position empty plastic bags on both sides of the sample to hold it in its proper place. After the plastic straw is mounted to the sample rod, the sample rod is inserted into the dewar. The sample rod is positioned so that every film has the applied magnetic field parallel to its surface, in other words, and in-plane magnetization measurement. Accumulation of hysteresis measurements with the MPMS system is rather easy because, once the sample is mounted and

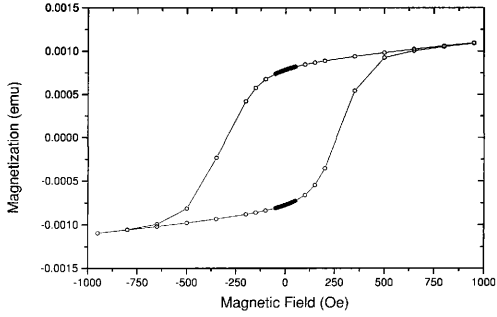

Fig. 6. Magnetization *vs* Magnetic Field at 10 K for film A16.

the appropriate conditions are entered into the computer, the system can operate by itself.

All of the ferromagnetic thin film hysteresis loops were measured. Figures 6 and 7 show magnetization as a function of magnetic field for films A16 and A20, whose thicknesses are 260 Å and 250 Å, respectively. The coercive force H_{cf}, or coercivity, is defined as the amount of reverse applied magnetic field that reduces the magnetization to zero. The large coercivities in films A16 and A20 are attributed to the Néel $t^{-4/3}$ dependence of H_{cf} [15], where t is the thickness of the film. Figures 8 and 9 exhibit hysteresis for film A19. Figure 9 is presented in order to reveal the low coercivity behavior of this film.

A film thickness almost twice as large, approximately 490 Å, is responsible for the decrease in coercivity. Similar behavior is demonstrated in Figures 10 and 11. Film A9, $t \approx 1120$ Å, is a good quality film with a coercive force $H_{cf} \approx 10$ Oe. A final plot of magnetization as a function of magnetic field is shown in Figure 12. This thin film, $t \approx 175$ Å, reveals a large coercive force similar to films A16 and A20. Figure 13 delineates the dependence of the coercive force on film thickness. The solid line represents an

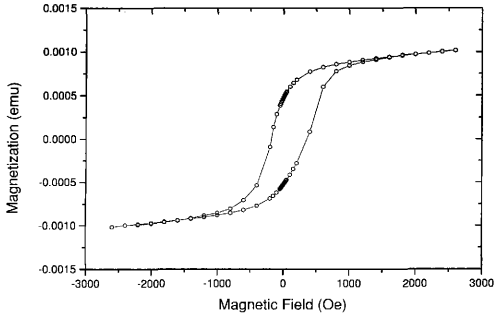

Fig. 7. Magnetization *vs* Magnetic Field at 10 K for film A20.

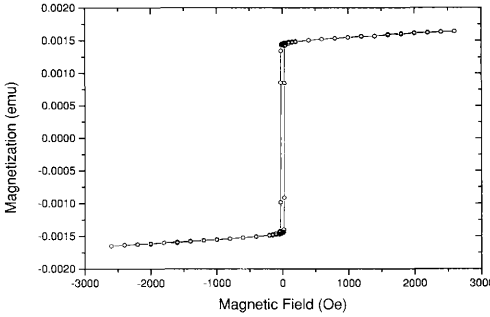

Fig. 8. Magnetization *vs* Magnetic Field at 10 K for film A19.

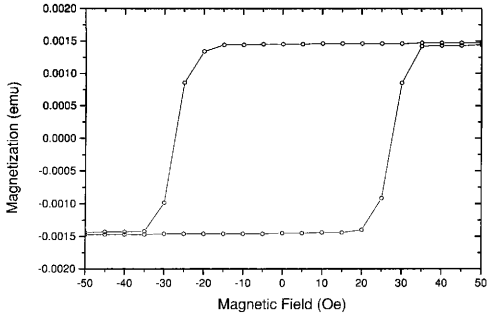

Fig. 9. Magnetization *vs* Magnetic Field at 10 K for film A19. This is plotted on a smaller scale to reveal the low coercivity behavior of this film.

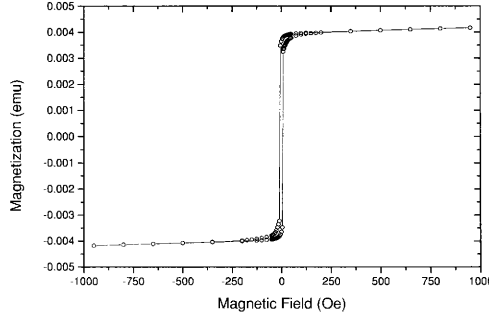

Fig. 10. Magnetization *vs* Magnetic Field at 10 K for film A9.

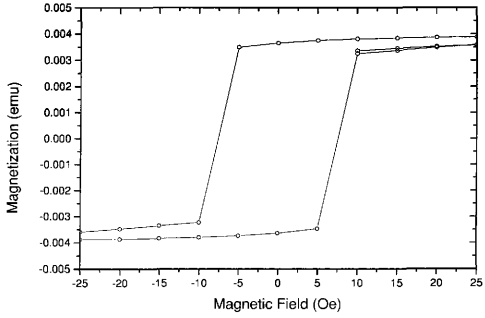

Fig. 11. Magnetization *vs* Magnetic Field at 10 K for film A9. This is plotted on a smaller scale to reveal the low coercivity behavior of this film.

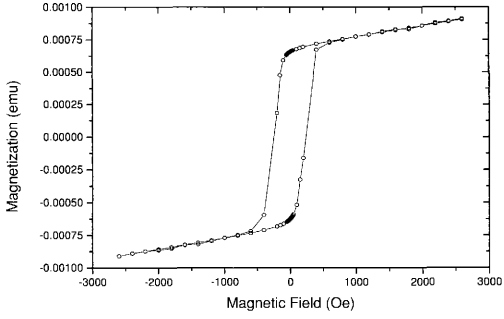

Fig. 12. Magnetization *vs* Magnetic Field at 10 K for film A21.

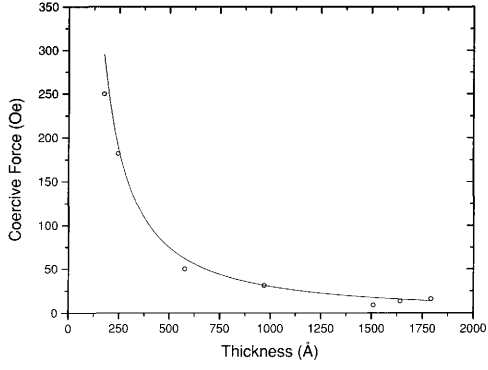

Fig. 13. Coercive Force *vs* Thickness for films A11, A13, A14, A15, A18, A20, and A21. The solid line represents a data fit according to the equation $H_{cf} = at^b$, where a is a constant and $b = 1.31076 \pm 0.3566$.

allometric fit of the experimental data. Fitting to the equation $H_{cf} = at^b$ yields a value of $b = -1.31076 \pm 0.3566$, which is very close to Néel's prediction that $H_{cf} \propto t^{-4/3}$.

Overall, most of the Co_xB_{1-x} thin films displayed hysteresis curves typical of soft magnetic materials. Small additions of Ge and Al did not reduce the coercivity when compared to the Co_xB_{1-x} thin films. The preparation and characterization of ferromagnetic thin films slowly transitioned into learning how to prepare and characterize superconducting thin films.

B. Superconducting Thin Films

Learning how to properly evaporate ferromagnetic thin films using the technique of flash evaporation made the evaporation of the superconducting thin films seem trivial, although it did require the same amount of time. The preparation and characterization of the superconducting thin films presented both triumphs and challenges as my project progressed.

1. Film Preparation

Evaporating the alloy $Pb_{95}Bi_5$ produced all of the superconducting thin films. Because Pb has a relatively high superconducting transition temperature, $T_c = 7.18$ K, it was chosen as the material to use in fabricating the superconducting thin films. Five atomic percent Bi introduces impurities that will increase the London penetration depth λ_L. The $Pb_{95}Bi_5$ alloys were prepared in a 95% Ar, 5% H atmosphere arc furnace using the appropriate atomic proportions of ultra pure Bi shot, 99.999%, and Pb foil. Melting and remelting the alloys ensured their uniformities. Compared to arc melting the Co_xB_{1-x} alloys, the $Pb_{95}Bi_5$ alloys were much easier to melt. Once the $Pb_{95}Bi_5$ sample was uniform, it was cut into small pieces using a sharp knife or wire cutters.

Due to such a small atomic percentage of Bi, the technique of flash evaporation is not required. So little Bi is present that the uniformity of the film is not compromised by not employing flash evaporation. When adapting the bell jar in order to evaporate $Pb_{95}Bi_5$ thin films, the material was placed directly into the 0.125" deep dimple of a W boat. After placing the desired amount material into the boat, two glass substrates approximately $0.5" \times 0.5"$ are set into the Al substrate holder with a brass mask patterned for standard four terminal technique measurements. In the case of evaporating the superconducting $Pb_{95}Bi_5$, the Al substrate holder is positioned at a height comparable to that of the quartz crystal monitor; therefore, no scaling factor is needed when calculating the approximate thickness

of the films.

Before evaporation, the quartz crystal monitor must be programmed accordingly. For the $Pb_{95}Bi_5$ alloy, $\rho = 11.3$ g/cm^3, Z-ratio = 1.130, and tooling = 100.0. Upon baking the vacuum system for at least 20 hours, the system reaches a pressure of $\sim 2 - 6 \times 10^{-7}$ torr and the evaporation can begin. Typically, passing 150 A of current through the W boat provided enough resistive heating to evaporate the material. This was difficult to determine in the first few evaporations of $Pb_{95}Bi_5$ because I had no idea about the relationship between current and evaporation rate for this particular alloy. After a few evaporations, I concluded that 150 A of current produced the desired evaporation rate. When evaporating the last two sets of thin films, a shutter was used during the initial stages of evaporation to ensure uniformity of the film. The shutter is attached to a rod that has a feedthrough which is subsequently attached to a handle that is outside of the bell jar. Once a steady evaporation rate is established, the shutter is rotated and the resulting vapor is allowed to strike the surface of the substrate. Use of the rotating shutter produced better quality $Pb_{95}Bi_5$ thin films.

Very few superconducting thin films were fabricated. Table II lists some of the different characteristics of the superconducting $Pb_{95}Bi_5$ thin films. These films were certainly easier to evaporate; however, producing a film which was electrically continuous proved difficult at first. This is a result of the films being too thin. To check continuity of the films, I applied Silver Print to the leads of one of each pair of the films. A standard multimeter was used in measuring the resistance across the film. All the films with $t \leq 1000$ Å were not continuous. Although Table II shows two films having $t > 1000$ Å, both of these films were not continuous either. This is probably due to some type of shadowing effect during the evaporations.

Time and availability of experimental equipment limited the production and characterization of the superconducting thin films. None of the six $Pb_{95}Bi_5$ thin films were charac-

Table II. Different characteristics of superconducting thin films. t_{cm} is the thickness of the film as determined by the quartz crystal monitor, RT indicates that the substrates were at room temperature during evaporation, LNT indicates that the substrates were at liquid nitrogen temperature during evaporation.

Alloy	Film	Base Pressure (torr)	t_{cm} (Å)	RT	LNT
$Pb_{95}Bi_5$	D1	1.1×10^{-6}	N/A	yes	no
$Pb_{95}Bi_5$	D2	6.0×10^{-7}	1970	yes	no
$Pb_{95}Bi_5$	D3	5.6×10^{-7}	1630	yes	no
$Pb_{95}Bi_5$	D4	2.7×10^{-7}	570	yes	no
$Pb_{95}Bi_5$	D5	2.8×10^{-7}	330	yes	no
$Pb_{95}Bi_5$	D6	3.4×10^{-7}	800	yes	no

terized by measuring resistance as a function of temperature. This would have determined the critical temperature T_c and given us some sort of idea whether or not the films were of suitable quality. Although dissatisfied with not being able to investigate the properties of the superconducting $Pb_{95}Bi_5$ thin films more rigorouly, I began fabrication of the SC/FM multilayer samples. With respect to the SC/FM samples, many $Pb_{95}Bi_5$ thin films were properly characterized.

CHAPTER III

THE SC/FM THIN FILM MULTILAYER

The fabrication and characterization of the SC/FM film couples comprised the most demanding and arduous work during the tenure of my thesis project. Many special parts were designed and machined in order to manufacture and measure certain characteristics of the SC/FM thin films. After overcoming many barriers, the samples were fabricated and characterized.

A. SC/FM Thin Film Multilayer Preparation

New ingots of both $Co_{61}B_{39}$ and $Pb_{95}Bi_5$ were melted in a 95% Ar, 5% H atmosphere in the arc furnace to produce the ferromagnetic and superconducting materials that will comprise the majority of the SC/FM film couple. I melted both samples three times to guarantee uniformity. After both samples were complete, the $Co_{61}B_{39}$ alloy was crushed into tiny particles and the $Pb_{95}Bi_5$ sample was cut into small particles. One millimeter diameter high purity Al and Ag wires were used for preparation of the oxide barrier and electrical leads, respectively. Both the Al and Ag wires were cut into approximately 0.5 cm pieces.

The first stage of manufacturing a SC/FM film couple is to evaporate the appropriate ferromagnetic thin film. Before evaporating the $Co_{61}B_{39}$ thin film, I attach the 0.008" thick brass mask, displayed in Figure 14, to the Al substrate holder shown in Figure 15 with two #2-56 hex screws. This mask is used to pattern the ferromagnetic thin film onto the substrate. After the mask is securely mounted onto the Al substrate holder, one 0.590" $\times$ 0.590" quartz substrate is placed into the Al substrate holder so that it rests on the mask. In addition to the quartz substrate, one 0.5" $\times$ 0.175" glass substrate is glued to the Al substrate holder using dilute GE varnish. The resulting film on the glass substrate is used for hysteresis measurements. Before fastening the substrate holder to the stainless

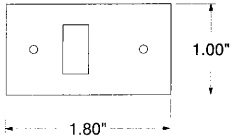

Fig. 14. Scale drawing of the mask used to pattern the ferromagnetic thin film onto the substrate.

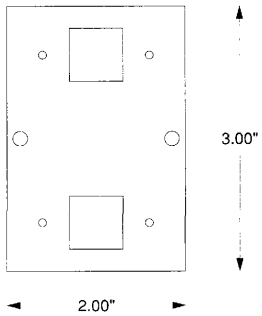

Fig. 15. Scale drawing of the aluminum substrate holder.

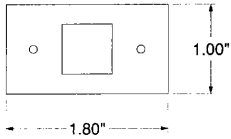

Fig. 16. Scale drawing of the mask used to pattern the oxide barrier.

steel rods in the bell jar, I retrieve the tiny particles of $Co_{61}B_{39}$ and place them into the holes of the slider. Once the Cu rod is aligned over the W boat and the substrate holder mounted to the stainless steel rods, the bell jar is closed and pumping begins. Baking the system for at least 24 hours yields pressures of $\sim 2 - 4 \times 10^{-7}$ torr. When a low pressure is attained, the $Co_{61}B_{39}$ is flash evaporated onto the quartz substrate producing a ferromagnetic thin film in the desired pattern.

Evaporation of an oxide insulation layer atop the $Co_{61}B_{39}$ thin film is the next step in the making of the SC/FM multilayer. After removing the substrate holder from the bell jar, the previously evaporated films are removed and set aside. Because the insulation barrier must cover the entire surface of the substrate, a new mask is used. Figure 16 shows the brass mask used to pattern the oxide barrier. The same quartz substrate with the ferromagnetic thin film evaporated onto it is placed inside the substrate holder and onto the new mask. Before it is mounted into the bell jar, the previous W boat is replaced by a W spiral basket. Four to five tiny Al horseshoe shaped wire pieces are situated on the outer perimeter of the spiral basket. Only a small amount of Al is placed on the spiral basket because the desired film thickness varies between 20 Å and 60 Å. As with the superconducting thin films, the substrate holder is positioned at a height comparable to that of the quartz crystal detector. Before the evaporation can take place, the quartz crystal detector must read $\rho = 2.70$ g/cm^3,

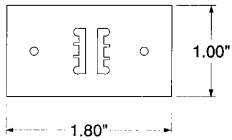

Fig. 17. Scale drawing of the mask used to pattern the superconducting thin films onto the oxide barrier.

Z-ratio = 1.080, and tooling = 100.0. The evaporation occurs using 30 - 40 A of current at base pressures of $\sim 1 - 5 \times 10^{-6}$ torr. The evaporation of Al does not take as much time as the other evaporations because we want the Al to oxidize, forming Al_2O_3, therefore pressures on the order of 10^{-7} torr are unnecessary. At a rate of 2 - 4 Å/s, a uniform Al thin film is fabricated. According to the quartz crystal monitor, typical Al film thicknesses vary between 30 Å and 40 Å. Upon opening the system to atmosphere, the Al thin film oxidizes and becomes Al_2O_3. The quartz substrate, now entirely coated with a thin Al_2O_3 barrier, is ready to have the superconducting thin films evaporated onto it.

The third step in manufacturing the SC/FM film couple consists of evaporating two superconducting $Pb_{95}Bi_5$ thin films onto the Al_2O_3 barrier. Figure 17 shows the brass mask adopted to pattern the superconducting films. Notice that both of the $Pb_{95}Bi_5$ films are deposited onto the Al_2O_3 barrier, but one is away from the ferromagnetic film while the other is positioned over the ferromagnetic thin film. It was designed in this manner in order to simultaneously measure the resistance as a function of temperature for two nearly identical superconducting thin films, one without the magnetic film and one with it. In this way, the interplay between the superconducting and ferromagnetic thin films can be compared to a nearly identical superconductor without a magnetic thin film. The superconducting film

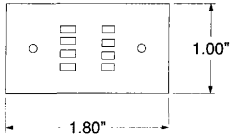

Fig. 18. Scale drawing of the mask used to pattern the Ag leads.

that is evaporated over the ferromagnetic film of the SC/FM sample is relatively centered with respect to the ferromagnetic thin film. This avoids any fringe magnetic fields that may exist at the edges of the film. The design of the mask also ensures that the distance between the two superconducting thin films is large enough so that the isolated superconductor does not experience any magnetic fields associated with the magnetic film. The evaporation of $Pb_{95}Bi_5$ onto the twice coated quartz substrate is executed following the same procedure previously discussed. Careful attention was exuded to the amount of material placed in the W boat because too little material would result in a discontinuous film. After successfully evaporating the two $Pb_{95}Bi_5$ thin films onto the Al_2O_3 barrier, electrical connections were applied to the superconducting thin films.

Electrical leads must exist to pass a current through a sample and subsequently measure its voltage. The chosen method to attack the problem of attaching leads to the unfinished SC/FM sample was to simply evaporate Ag for the electrical leads. Figure 18 shows the brass mask utilized to pattern the Ag leads. The design of the mask allows a portion of each small rectangular Ag film to overlap the small extensions of the superconducting thin films, thereby establishing a connection through which current can flow. The evaporation of Ag is rather easy, but still requires the same amount of time when compared to the evaporations of $Co_{61}B_{39}$ and $Pb_{95}Bi_5$. A small piece of 1.0 mm diameter Ag wire is placed into

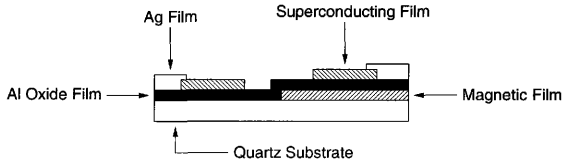

Fig. 19. Idealized cross-section of finished SC/FM film couple. The thickness of the Al film is exaggerated.

either a tantalum or molybdenum boat. No scaling factor is needed because I positioned the substrate holder at nearly the same height as the crystal monitor. For the evaporation of Ag, $\rho = 10.5$ g/cm^3, Z-ratio = 0.529, and tooling = 100.0. Passing a current of approximately 140 A melted the Ag wire and the resulting vapor formed the Ag leads of the SC/FM film couple. A finished SC/FM thin film multilayer existed after the evaporation of the Ag electrical leads. Figure 19 shows an idealized cross-section of a completed SC/FM sample.

It took approximately four to five days to fabricate a complete SC/FM film couple. Table III shows some of the different characteristics of the SC/FM samples. Characterization of the SC/FM samples followed their preparation.

B. SC/FM Thin Film Multilayer Characterization

Characterization of the samples involved measuring resistance as a function of temperature in a range of magnetic fields between 0 G and 2 kG. The measure of a sample's opposition to the flow of charge carriers through the sample is known as resistivity. Resistance, which depends on the dimensions of the sample, is related to the resistivity by the equation

$$R = \rho \frac{L}{A},$$

Table III. Different characteristics of the SC/FM film couples. t_m is the magnetic thin film thickness, t_{Al} is the Al thin film thickness, t_{sc} is the superconducting thin film thickness, t_{Ag} is the Ag thin film thickness. All film thicknesses are approximate.

Sample	t_m (Å)	t_{Al} (Å)	t_{sc} (Å)	t_{Ag} (Å)
SC/FM1	1040	30	1900	550
SC/FM2	490	35	1900	550
SC/FM3	1570	30	750	600
SC/FM4	300	40	1200	570

where R is the resistance, ρ is the resistivity, L is the length of the sample, and A is the cross-sectional area of the sample perpendicular to the charge carrier flow. Resistivity is a useful transport property to study in order to determine the behavior of charge carriers in a material. Measuring resistance as a function of temperature with the sample in a magnetic field yields information on whether or not the magnetic thin film is effectively pinning vortices in the superconductor. This measurement also reveals the effect of the magnetic field on the critical temperature T_c.

Resistance was measured using the standard four terminal technique. In this technique, current is passed through a sample via two outer terminals, with the remaining terminals used to measure the voltage difference across the sample. Using Ohm's Law, $V = IR$, the resistance is easily calculated. Figure 20 shows the basic idea of measuring the voltage across a SC/FM sample. Current is passed through the sample via the outer Ag films, while the voltage difference is measured across the two inner Ag films. For all of the SC/FM samples, a current of 10 μA was used.

Many special parts were designed and machined in order to measure the SC/FM samples using the four terminal technique. Before the samples could be mounted into the ^{4}He

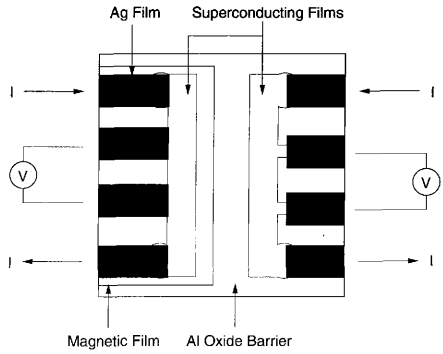

Fig. 20. Measuring voltage of a SC/FM sample.

cryostat, two 0.125" thick circular Cu sample holders were machined specifically to accomodate the size of the sample. To establish a dc current through the superconducting thin film and subsequently measure its voltage, tiny Ag pads were pressed onto the rectangular Ag films of the SC/FM sample using small Teflon pieces [1]. Figure 21 shows how the Ag pads are clamped onto the SC/FM film couple. For every substrate, *i.e.* two superconducting films, one with a ferromagnetic thin film and one without, two pairs of Teflon pieces were used. Since two pairs of Teflon pieces were needed for each substrate, and four samples were measured, sixteen Teflon pieces were machined. The Teflon pieces are attached to the Cu sample holders using #0-80 screws. Each pair of Teflon pieces clamp four Ag foils onto one of the superconducting thin films of the SC/FM sample. On the other side of a Teflon pair, 0.003" diameter Cu wires were In soldered to each of the Ag foils, as shown

[1] Teflon is a registered trademark of DuPont

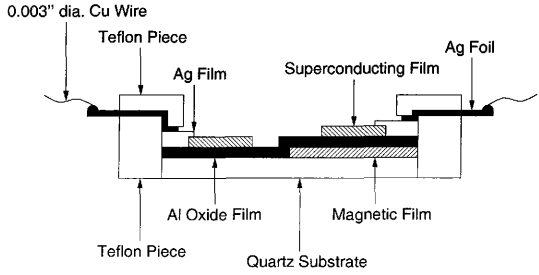

Fig. 21. Clamping Ag foils onto the SC/FM sample. The thickness of the Al film is exaggerated.

in Figure 21. Because each film required four leads, and there were a total of eight films, 32 Cu wires were soldered to the tiny Ag foils. This was a very tedious task due to the tiny diameter of the Cu wire and small area of the Ag foil. The Cu wire allows a current to be passed into the Ag foil, continuing through the Ag film, and eventually reaching the superconducting thin film. This current flows through the superconductor and exits in the reverse order. Similarly, a voltage is measured across the sample as a current is supplied.

Before the samples and sample holders are ready to be mounted in the ^{4}He cryostat, the opposite ends of the wires must be In soldered into 7 pin connectors, which are subsequently connected to various meters that lie outside the cryostat and dewar. Once the SC/FM samples are secured to the Cu sample holders and the wires properly soldered into the 7 pin connectors, they are mounted into a ^{4}He cryostat. After the ^{4}He cryostat is placed into the dewar and cooled down, measurements can begin.

1. The ^{4}He cryostat and Related Equipment

All four SC/FM samples were mounted in a 1 K pot ^{4}He cryostat. The 1 K pot refers to a pot of liquid ^{4}He that allows the samples to reach a temperature near 1 K when the liquid ^{4}He is pumped. Figure 22 shows the dewar with the cryostat mounted inside. The distance from the bottom of the dewar to the top of the mounted ^{4}He cryostat is approximately 7.5', with the cryostat itself measuring 6' in length. Conduction, convection, and radiation heat leaks are minimized to allow the cryostat to remain at stable temperatures between 4.2 K - 300 K [16]. See Reference [16] for a more detailed discussion of the ^{4}He cryostat.

The SC/FM samples are easy to mount in the cryostat if both the vacuum and sample cans are unscrewed and removed. Figure 23 shows the sample can. Both sample holders are attached to the Cu mounting block using two 2" long brass screws. Because the applied magnetic field is always perpendicular to the samples in this particular setup, it is very important that the screws are tight so that the samples are as close to normal as possible. Once the 7 pin connectors are plugged into their appropriate sockets, the In o-ring is made and used to seal the sample can to a stainless steel flange. A heater which is wrapped in a helical fashion around the sample can is then plugged into another connector. To maintain equilibrium between the sample can and sample plug, a thin Cu sheath is placed around the sample can and firmly tied to it using waxed dental floss. The Cu sheath serves as a thermal conductor between the sample can and sample plug. Figure 24 shows the vacuum can that contains the 1 K pot and sample can. The vacuum can, like its tenant the sample can, is attached to a stainless steel flange using an In o-ring. After the vacuum can is tightened to the flange, the cryostat is lowered into the super insulated dewar made by Precision Cryogenics Systems Inc.

Since the superconducting magnet was used, liquid nitrogen (LN_2) was transferred to both the magnet space and the vacuum can space. After filling both spaces with LN_2, it

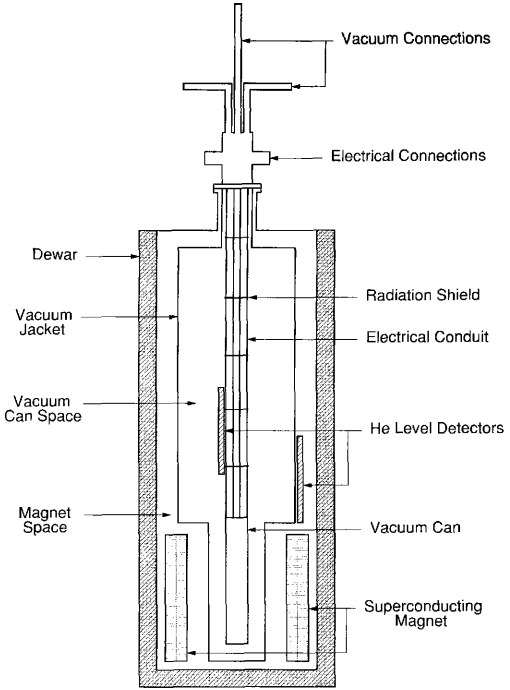

Fig. 22. Drawing of the cryostat in the dewar.

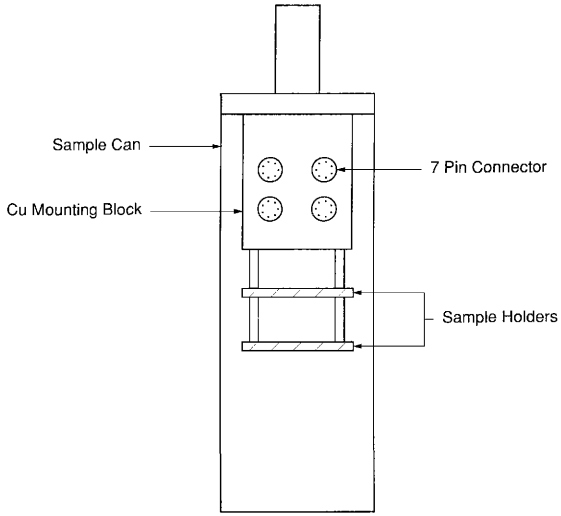

Fig. 23. Drawing of the sample can.

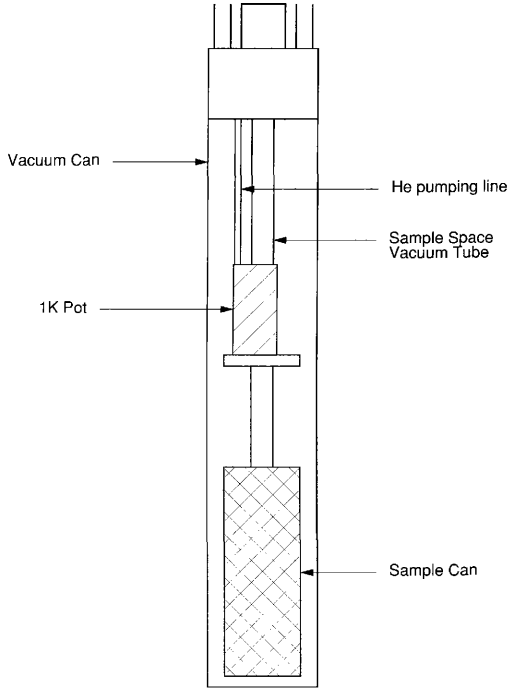

Fig. 24. Drawing of the vacuum can.

takes the samples approximately a day to cool down to LN_2 temperature, which is 77 K. Because LN_2 is inexpensive, it is used to pre-cool the samples and magnet so that when liquid helium (LHe) is tranferred, not as much is required to cool to 4.2 K. A Kinney pump is used to pump out any residual N_2 gas. Liquid helium is then transferred to both the magnet space and the vacuum can space. This allows both spaces to reach LHe temperature, or 4.2 K.

Two triple current power supplies performed many important functions. Each power supply contains three constant current sources. Subsequently, each current source contains seven stages, with the lowest and highest stages supplying 0.1 μA and 100 mA of current, respectively. These constant current sources provided current for the samples, the carbon-glass resistance thermometer, and the persistent current switch for the superconducting magnet. A separate constant current source controls the cernox temperature sensor. Both the cernox and carbon-glass resistors serve as thermometers for the samples. They are located on a Cu block that lies just above the stainless steel flange of the sample can. The temperature is determined by measuring the voltage difference across either of the calibrated thermometers. Because the current source for the cernox sensor only produces a voltage difference of 1 - 3 mV, it is generally the sensor used to measure the temperature of the samples from room temperature to LHe temperature. The current source for the carbon-glass resistor generates a voltage difference of 1 - 12 mV, ergo it is used for for measuring the temperature near or below LHe temperature.

An American Magnetics 2385 superconducting magnet generates the magnetic field needed to measure magnetoresistance. Figure 22 shows the position of the magnet with respect to the dewar and cryostat. A Hewlett-Packard 6260B DC Power Supply provided the current for the superconducting magnet. Similarly, an American Magnetics, Inc. Programmer, Model 400A, controlled the amount of current in the magnet. To easily adjust the magnetic field, the persistent current switch must be operational. The persistent current

switch is a superconducting wire that is forced into the normal state by heating the wire. Since the persistent current switch lies in parallel with the superconducting magnet's coils, the change from zero resistance to full resistance due to the heating of the switch allows the magnetic field to be changed by a change in the current to the magnet coil applied by an external power supply.

Measuring the voltage across the samples required four voltmeters. The four voltmeters included three Keithley 181 Nanovoltmeters and one Keithley 196 System DMM voltmeter. Various other meters were used to measure the the strength of the magnetic field, temperature inside the magnet space, and the amount of LHe in both the magnet space and the vacuum can space.

All data was taken on a Macintosh Centris 650 using Labview Software. Once the SC/FM samples were cooled to LHe temperature, I started the program and it automatically retrieved the zero field data until it reached the desired temperature, which was around 10 K for my experiment. After the data run had completed, the samples recooled to approximately 4.2 K and were subjected to a magnetic field normal to the substrate. A new data file was started and allowed to finish. This process was repeated for a range of magnetic fields between 0 G - 2 kG.

CHAPTER IV

RESULTS AND DISCUSSION

Hysteresis data was obtained for all of the SC/FM samples. Figures 25 and 26 display the magnetization as a function of magnetic field for sample SC/FM1. Inspection of Figure 26 reveals that $H_{cf} \approx 21$ Oe, which is a low coercivity for a magnetic thin film with an approximate thickness of 1040 Å. Two hysteresis curves for sample SC/FM2 are presented in Figures 27 and 28. It is shown in Figure 28 that $H_{cf} \approx 25$ Oe, which is slightly lower than many of the other $Co_{61}B_{39}$ ferromagnetic films fabricated around this thickness. An observant reader may notice that the hysteresis curve in Figure 28 is slightly shifted to the left, in other words, it is not symmetric about the origin. This is due to a residual magnetic field in the SQUID superconducting magnet. Sample SC/FM3 possesses the thickest ferromagnetic thin film, $t_m \approx 1570$ Å, where t_m denotes the thickness of the magnetic film. Its hysteresis curves are exhibited in Figures 29 and 30. From our previous discussion, it is not surprising that $H_{cf} \approx 17$ Oe is the lowest coercivity present. The highest coercive field belongs to sample SC/FM4, whose magnetization as a function of magnetic field is displayed in Figure 31. Its coercivity $H_{cf} \approx 200$ Oe is an order of magnitude greater than the other three samples, but this is expected since $t_m \approx 300$ Å. Table IV summarizes the magnetic thin film thicknesses and film coercivities for the SC/FM samples. Overall, the magnetic thin films were high quality films with low coercivities.

Sample SC/FM2 was the best sample of the four fabricated. Niether samples SC/FM1 or SC/FM4 yielded very good data, and sample SC/FM3, with a superconducting thin film thickness of $t_{sc} \approx 765$ Å, revealed no signs of continuity. Both the superconducting film coupled with the magnetic film and the superconducting film displayed promising data for sample SC/FM2. Sample SC/FM1 demonstrated nice characteristics for the coupled superconducting/magnetic films, but very strange behavior for the superconducting film. At the

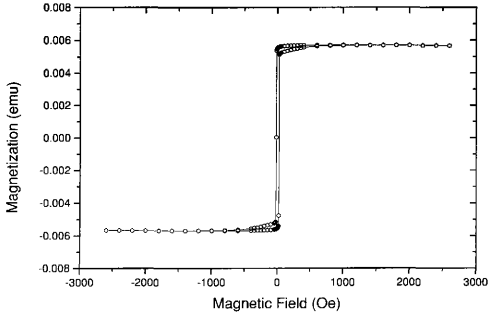

Fig. 25. Magnetization *vs* Magnetic Field at 10 K for sample SC/FM1.

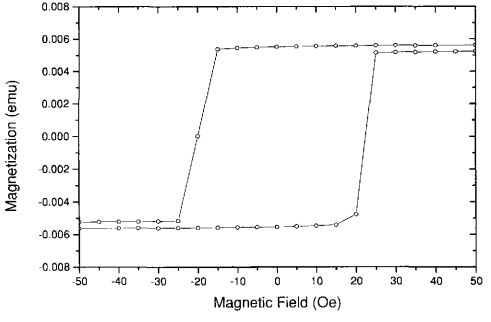

Fig. 26. Magnetization *vs* Magnetic Field at 10 K for sample SC/FM1. This is plotted on a smaller scale to reveal the low coercivity behavior of this film.

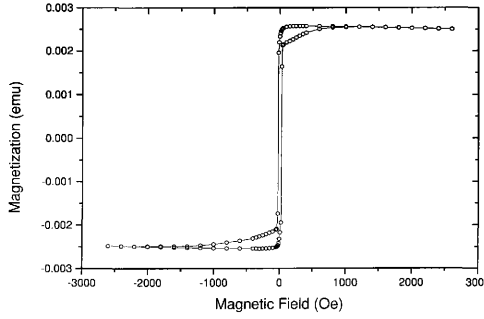

Fig. 27. Magnetization *vs* Magnetic Field at 10 K for sample SC/FM2.

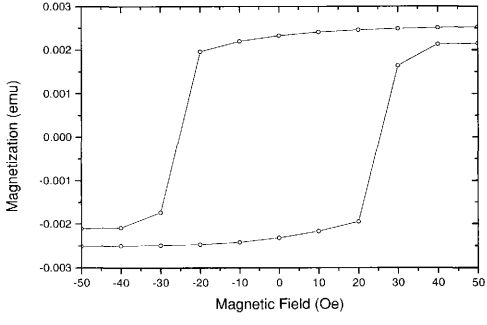

Fig. 28. Magnetization *vs* Magnetic Field at 10 K for sample SC/FM2. This is plotted on a smaller scale to reveal the low coercivity behavior of this film.

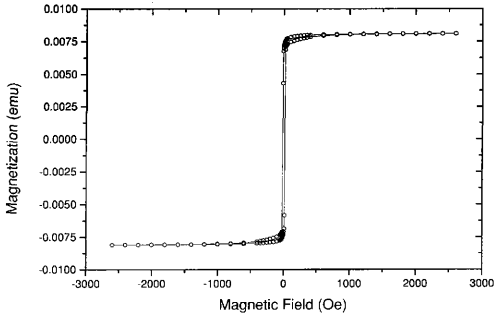

Fig. 29. Magnetization *vs* Magnetic Field at 10 K for sample SC/FM3.

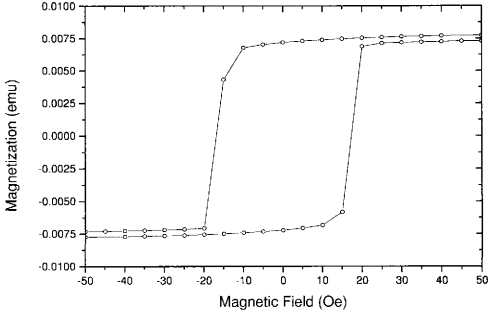

Fig. 30. Magnetization *vs* Magnetic Field at 10 K for sample SC/FM3. This is plotted on a smaller scale to reveal the low coercivity behavior of this film.

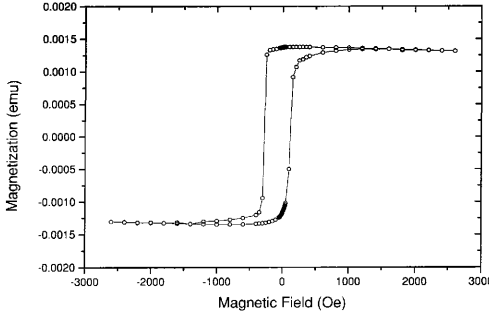

Fig. 31. Magnetization *vs* Magnetic Field at 10 K for sample SC/FM4.

Table IV. Magnetic thin film thicknesses and approximate coercive fields for the SC/FM samples. t_m is the magnetic thin film thickness, $\approx H_{cf}$ is the approximate coercivity.

Sample	t_m (Å)	$\approx H_{cf}$ (Oe)
SC/FM1	1040	21
SC/FM2	490	25
SC/FM3	1570	17
SC/FM4	300	200

superconducting transition temperature, the resistance of this sample began to rise linearly. This is probably due to a bad electrical connection or short to ground somewhere between the sample and 7 pin connector. The opposite is true for sample SC/FM4. Although there existed an anomalous kink at the onset of superconductivity, the superconducting film exhibited zero resistance below T_c. Nonetheless, the data for the superconductor with the magnetic film was very noisy. Because we are interested in comparing the behavior of the coupled superconducting/magnetic films with the behavior of an almost identical superconducting film, only sample SC/FM2 sufficed. All of the data presented hereafter is attributed to sample SC/FM2.

Since a voltage difference is measured across a sample, all of the accumulated data was divided by a current of 10 μA to retrieve the resistance of a sample. Figure 32 shows the resistance as a function of temperature at $H_c = 500$ G for the superconducting thin film. It reveals a rather sharp transition with $T_c \approx 7$ K. This is presented to show that the superconducting thin film is indeed superconducting.

Figure 33 displays the normalized resistivity as function of temperature at $H_c = 0$ G. Normalizing the resistivity, or dividing the resistivity by the resistivity evaluated at some known temperature above T_c, is very useful in drawing conclusions about the data because any geometrical factors contributed by the sample cancel out. The superconducting film in zero field has a $T_c \approx 7.5$ K, which is approximately 0.3 K higher than the transition temperature for Pb, $T_c = 7.18$ K. The value of T_c is shifted by 0.3 K because as the data was collected, a leak existed in either the In o-ring seal of the sample can or the epoxy seals where electrical wiring enters the sample can. Because of this He exchange gas leak, the samples were at a lower temperature than the temperature of the carbon-glass resistance thermometer. As a result, the superconducting transition temperature is shifted for all of the normalized resistivities. Figure 33 also exposes the peculiar behavior of the superconducting film in the presence of the magnetic thin film. This film follows

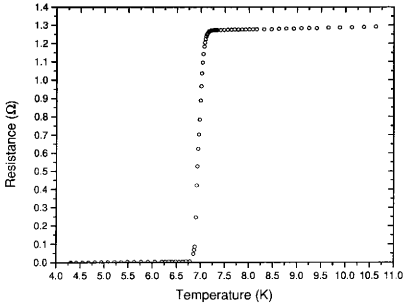

Fig. 32. Resistance *vs* Temperature at $H_c = 500$ G for the superconducting thin film of sample SC/FM2.

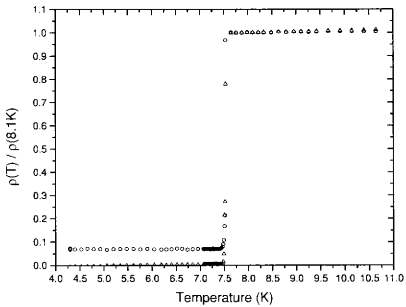

Fig. 33. Normalized resistivity *vs* Temperature at zero field for sample SC/FM2. The circles (○) represent the superconductor with the presence of a magnetic thin film; whereas, the triangles (△) represent the isolated superconductor.

a nearly identical transition to the superconducting film without a magnetic film, but the resistance drops to a constant nonzero value. We thought that this could be a result of the current shorting to the magnetic film. If the Ag foils were clamping down too tightly onto the sample, the Ag foils might have pressed through the Ag films and Al_2O_3 barrier to short the sample. This scenario would be equivalent to two resistors in parallel, where the resistors are the superconducting and magnetic films, respectively. This is not a plausible explanation though because even if both films were in parallel, as soon as sample reached T_c, the $Pb_{95}Bi_5$ film would go superconducting and all of the charge carriers would flow through that film, producing a net resistance of zero. Although no exact explanation exists at this point, the nonzero resistance is probably a result of poor pressure contacts or inferior electrical connections.

Figures 34, 35, 36, 37, 38, 39, and 40 show the normalized resistivities as functions of temperature for $H_c = 250$ G, 500 G, 750 G, 1 kG, 1250 G, 1500 G, and 2 kG, respectively. As is the case at zero applied magnetic field, all of the coupled superconducting/magnetic films reduce to a nonzero value of resistance below T_c. Similarly, all of the superconducting films have zero resistance below T_c. As $H_c \neq 0$ increases, observe that the onset of superconductivity experienced by the superconducting film in the presence of the magnetic film occurs at a lower temperature. What is even more interesting is that as $H_c \neq 0$ increases, the differences in the onsets of superconductivity are increasing. Consider, for example, Figure 34. At a value of $\rho(T)/\rho(8.1\text{ K}) \approx 1$, the onset of superconductivity is only slightly less for the coupled superconducting/magnetic films. In Figure 39, the onset of superconductivity is noticeably less for the superconducting/magnetic system at $\rho(T)/\rho(7\text{ K}) \approx 1$. This sizeable difference leads us to believe that the presence of the magnetic film does have an effect on the behavior of the superconductor.

Figure 41 shows the dependence of the the critical magnetic field H_c on the superconducting transition temperature T_c. The BCS theory of superconductivity predicts that

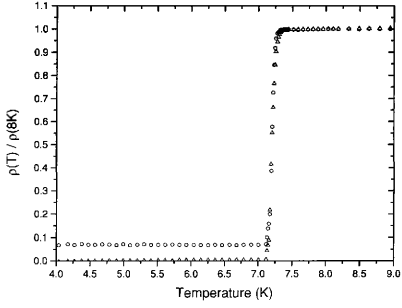

Fig. 34. Normalized resistivity *vs* Temperature at $H_e = 250$ G for sample SC/FM2. The circles (◯) represent the superconductor with the presence of a magnetic thin film; whereas, the triangles (△) represent the isolated superconductor.

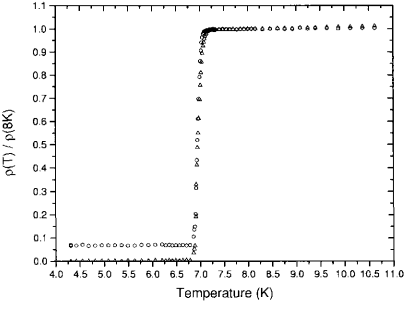

Fig. 35. Normalized resistivity *vs* Temperature at $H_e = 500$ G for sample SC/FM2. The circles (◯) represent the superconductor with the presence of a magnetic thin film; whereas, the triangles (△) represent the isolated superconductor.

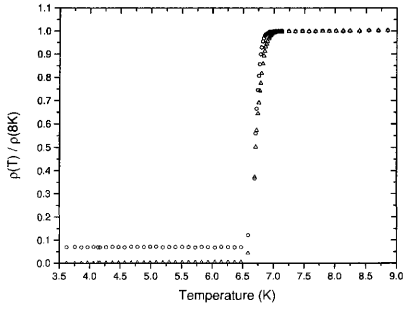

Fig. 36. Normalized resistivity *vs* Temperature at $H_c = 750$ G for sample SC/FM2. The circles (◯) represent the superconductor with the presence of a magnetic thin film; whereas, the triangles (△) represent the isolated superconductor.

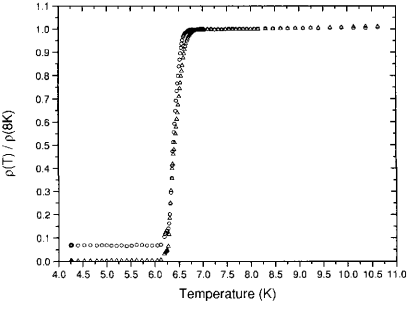

Fig. 37. Normalized resistivity *vs* Temperature at $H_c = 1$ kG for sample SC/FM2. The circles (◯) represent the superconductor with the presence of a magnetic thin film; whereas, the triangles (△) represent the isolated superconductor.

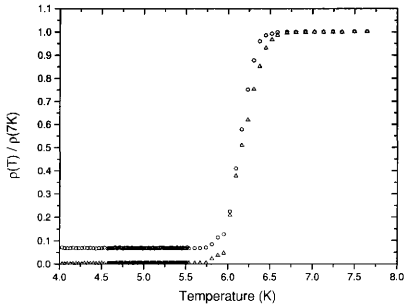

Fig. 38. Normalized resistivity *vs* Temperature at $H_c = 1250$ G for sample SC/FM2. The circles (◯) represent the superconductor with the presence of a magnetic thin film; whereas, the triangles (△) represent the isolated superconductor.

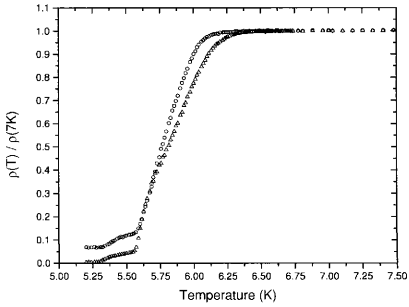

Fig. 39. Normalized resistivity *vs* Temperature at $H_c = 1500$ G for sample SC/FM2. The circles (◯) represent the superconductor with the presence of a magnetic thin film; whereas, the triangles (△) represent the isolated superconductor.

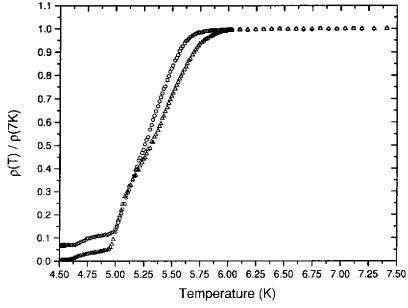

Fig. 40. Normalized resistivity *vs* Temperature at $H_c = 2$ kG for sample SC/FM2. The circles (◯) represent the superconductor with the presence of a magnetic thin film; whereas, the triangles (△) represent the isolated superconductor.

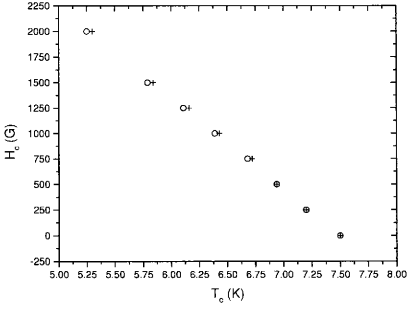

Fig. 41. Critical magnetic field H_c *vs* superconducting transition temperature T_c for sample SC/FM2. The circles (◯) represent the superconductor with the presence of a magnetic thin film; whereas, the crosses (+) represent the isolated superconductor.

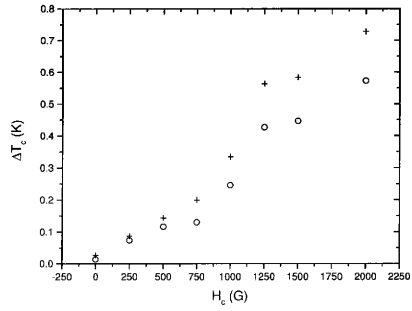

Fig. 42. The superconducting transition width ΔT_c plotted against the critical magnetic field H_c for sample SC/FM2. The circles ($\bigcirc$) represent the superconductor with the presence of a magnetic thin film; whereas, the crosses ($+$) represent the isolated superconductor.

$H_c(T)$ is governed by the approximate relation $H_c(T)/H_c(0) \approx 1 - (T/T_c)^2$. Although the data is relatively linear, it does maintain a negative slope. There is also a slight departure in T_c between the superconducting/magnetic films and the superconducting film as H_c increases.

The superconducting transition width ΔT_c is plotted against the critical field H_c in Figure 42. Consider the normalized resistivities presented in Figure 38. Let $\rho(T_1)/\rho(7\ \mathrm{K}) \approx 0.9$ and $\rho(T_2)/\rho(7\ \mathrm{K}) \approx 0.2$ for one particular curve. The superconducting transition width is $T_1 - T_2 \equiv \Delta T_c$. It is clear from Figure 42 that as H_c increases, ΔT_c increases as well. This is consistent with the behavior of type II superconductors. As H_c increases, more magnetic flux penetrates the film. Recall that every fluxon penetrating the sample does so through a normal core. Since H_c is increasing, more normal cores are threading the film, which results in an increase in the flux flow resistance. The growth in flux flow resistance

broadens the superconducting transition width. This trend is apparent in both the coupled superconducting/magnetic films and the isolated superconducting film.

Figure 42 also reveals interesting behavior in that for every value of H_c, ΔT_c is smaller for the coupled SC/FM films than for the isolated superconducting film. A smaller ΔT_c indicates that the superconducting transition width has decreased. This affirms that the presence of a ferromagnetic thin film sharpens the superconducting transition. The sharpening of the superconducting transition signifies a reduction in the flux flow resistance. In other words, the interaction between the superconducting thin film and the ferromagnetic thin film results in the pinning of superconducting vortices.

CHAPTER V

CONCLUSION

The thrust of this research was to determine whether or not the interaction between a superconducting thin film and a ferromagnetic thin film separated by a thin insulating layer effectively pinned superconducting vortices, thereby reducing the flux flow resistance.

Although the results of this study are preliminary, they indeed suggest that the interaction between a superconducting thin film and a ferromagnetic thin film separated by a thin oxide layer results in the partial pinning of superconducting vortices, thus decreasing the flux flow resistance. This indicates that there may be a coupling between the superconducting vortices in the superconductor that are produced by the applied magnetic field and magnetic defects. The nature of the magnetic defects, whether grain boundaries, magnetic vortices, or some other type of defect, has not been established. No evidence was observed for spontaneous generation of coupled magnetic and superconducting vortices absent a magnetic field.

The possibilities for continuing this research are endless. Many different materials could possibly be studied in order to understand the behavior of the SC/FM thin film multilayer. Varying the thicknesses of the films and studying how the SC/FM system changes with changes in the nature of the insulation barrier also deserves attention.

Although this study was not exhaustive in terms of delineating the physics in this configuration of magnetically coupled magnetic and superconducting thin films, it demonstrated that interesting phenomena is present, and I have developed techniques that can be used to further study the problem. The intricate interplay between superconductivity and ferromagnetism is far from being completely understood; however, the only path towards understanding lies in the ability to do research, therefore the research continues.

REFERENCES

[1] V. L. Ginzburg, E. A. Andryushin, Superconductivity, World Scientific, Singapore, 1994.

[2] N. W. Ashcroft, N. D. Mermin, Solid State Physics, Harcourt Brace College Publishers, Fort Worth, 1976.

[3] B. S. Deaver, W. M. Fairbank, Phys. Rev. Lett. 7 (1961) 43.

[4] R. Doll, M. Näbauer, Phys. Rev. Lett. 7 (1961) 51.

[5] J. Bardeen, L. N. Cooper, J. R. Schrieffer, Phys. Rev. 108 (1957) 1175.

[6] L. N. Bulaevskii, A. I. Buzdin, M. L. Kulic, S. V. Panyukov, Adv. Phys. 34 (1985) 175.

[7] O. Fisher, Ferromagnetic Materials, Vol.5, North-Holland, Amsterdam, 1990.

[8] I. F. Lyuksyutov, D. G. Naugle, Physica C 341 - 348 (2000) 1267 - 1268.

[9] A. A. Abrikosov, L. P. Gorkov, Sov. Phys. JETP 12 (1961) 1243 - 1253.

[10] I. F. Lyuksyutov, D. G. Naugle, Mod. Phys. Lett. B 13 (1999) 491.

[11] R. F. Soohoo, Magnetic Thin Films, Harper & Row, New York, 1965.

[12] J. E. Mahan, Physical Vapor Deposition of Thin Films, Wiley, New York, 2000.

[13] Thin Film Thickness & Rate Monitor, Model XTM, May 1979, Inficon.

[14] MPMS XL User's Manual, Quantum Design, San Diego, CA, 1996.

[15] L. Néel, J. Phys. Radium 17 (1956) 250.

[16] B. D. Hennings, Transport Properties of Metal-Oxide, High T_c Superconductors, Undergraduate Thesis, *1991-1992*.

VITA

Isaac John Sullivan was born May 16, 1979, to Mary Ann Yancy and David P. Sullivan in Dallas, TX. He is currently pursuing a B.S. degree in Physics as well as a B.S. degree in Pure Mathematics at Texas A&M University. Permanent contact: David P. Sullivan, 1105 Mayleaf Dr., Irving, TX 75060.

This document was typeset with LaTeX.